Dahm, T., Cesca, S., Hainzl, S., Braun, T., Krüger, F. (2015): Discrimination between induced, triggered, and natural earthquakes close to hydrocarbon reservoirs: A probabilistic approach based on the modeling of depletion-induced stress changes and seismological source parameters. - *Journal of Geophysical Research*, *120*, p. 2491-2509.

DOI: http://doi.org/10.1002/2014JB011778

AGU PUBLICATIONS

JGR

Journal of Geophysical Research: Solid Earth

RESEARCH ARTICLE

10.1002/2014JB011778

Key Points:
- Novel probabilistic discrimination for induced, triggered, and natural EQ
- Demonstrate method with three applications
- Study is of relevance to academia, industry, and public

Correspondence to:
T. Dahm,
torsten.dahm@gfz-potsdam.de

Citation:
Dahm, T., S. Cesca, S. Hainzl, T. Braun, and F. Krüger (2015), Discrimination between induced, triggered, and natural earthquakes close to hydrocarbon reservoirs: A probabilistic approach based on the modeling of depletion-induced stress changes and seismological source parameters, *J. Geophys. Res. Solid Earth*, *120*, 2491–2509, doi:10.1002/2014JB011778.

Received 17 NOV 2014
Accepted 5 MAR 2015
Accepted article online 10 MAR 2015
Published online 13 APR 2015

Discrimination between induced, triggered, and natural earthquakes close to hydrocarbon reservoirs: A probabilistic approach based on the modeling of depletion-induced stress changes and seismological source parameters

Torsten Dahm[1,2], Simone Cesca[1,2], Sebastian Hainzl[1], Thomas Braun[3], and Frank Krüger[2]

[1]GFZ German Research Centre for Geosciences, Potsdam, Germany, [2]Institut für Erd- und Umweltwissenschaften, Universität Potsdam, Germany, [3]Istituto Nazionale di Geofisica e Vulcanologia, Seismology & Tectonophysics, Arezzo, Italy

Abstract Earthquakes occurring close to hydrocarbon fields under production are often under critical view of being induced or triggered. However, clear and testable rules to discriminate the different events have rarely been developed and tested. The unresolved scientific problem may lead to lengthy public disputes with unpredictable impact on the local acceptance of the exploitation and field operations. We propose a quantitative approach to discriminate induced, triggered, and natural earthquakes, which is based on testable input parameters. Maxima of occurrence probabilities are compared for the cases under question, and a single probability of being triggered or induced is reported. The uncertainties of earthquake location and other input parameters are considered in terms of the integration over probability density functions. The probability that events have been human triggered/induced is derived from the modeling of Coulomb stress changes and a rate and state-dependent seismicity model. In our case a 3-D boundary element method has been adapted for the nuclei of strain approach to estimate the stress changes outside the reservoir, which are related to pore pressure changes in the field formation. The predicted rate of natural earthquakes is either derived from the background seismicity or, in case of rare events, from an estimate of the tectonic stress rate. Instrumentally derived seismological information on the event location, source mechanism, and the size of the rupture plane is of advantage for the method. If the rupture plane has been estimated, the discrimination between induced or only triggered events is theoretically possible if probability functions are convolved with a rupture fault filter. We apply the approach to three recent main shock events: (1) the M_w 4.3 Ekofisk 2001, North Sea, earthquake close to the Ekofisk oil field; (2) the M_w 4.4 Rotenburg 2004, Northern Germany, earthquake in the vicinity of the Söhlingen gas field; and (3) the M_w 6.1 Emilia 2012, Northern Italy, earthquake in the vicinity of a hydrocarbon reservoir. The three test cases cover the complete range of possible causes: clearly "human induced," "not even human triggered," and a third case in between both extremes.

1. Introduction

The problem of induced and triggered earthquakes and the discrimination between natural and human-related earthquakes is old. Already in 1908 the first local seismic network was established in Bochum in the Ruhr area, Germany, to monitor possible induced earthquakes related to coal mining [see, e.g., *McGarr et al.*, 2002]. Since then, stronger events induced or triggered by coal mining in Germany reached magnitudes of M_L 4.2 [e.g., *Cesca et al.*, 2013a; *Dahm et al.*, 2010, and references therein]. The most severe induced earthquakes in Germany, however, were related to potash mining (M_L 5 Heringen/Widdernhausen 1953, M_L 5.2 Sünna/Werra 1975, M_L 5.5 Völkershausen 1989, and M_L 4.9 Teutschenthal/Halle 1996) [see *Grünthal and Minkley*, 2005, and references therein] and to conventional gas production (e.g., M_W 4.4 Rotenburg 2004 [see *Dahm et al.*, 2007]). Worldwide, even larger human-triggered earthquakes have been discussed, among which several $M > 6$ earthquakes include events in vicinity to hydrocarbon reservoirs (see, e.g., *McGarr et al.* [2002] for a historical review) and artificial water reservoirs (e.g., 1967 *M*6.3 Koyna earthquake, India [*Gupta*, 2002]). The possible human influence for such damaging earthquakes close to

geotechnical operations often leads to long disputes between seismologists, the public, and stakeholders from industry, especially since commonly accepted rules for the discrimination between human-induced and natural earthquakes do not actually exist.

In order to tackle the discrimination problem, usually, the temporal and spatial correlation of earthquakes to regions under geotechnical activities is investigated. If the event is "close enough" and "occurred within the period of human activity," it is assumed to be related to the activity. However, a clear definition of "closeness" or "period" is not established. Such a definition should consider, at least, the type and the size of the region affected by the geotechnical operation as well as the size of the rupture plane.

Another qualitative discrimination approach has been suggested by *Davis and Frohlich* [1993] for fluid injection and by *Davis et al.* [1995] for fluid withdrawal, where either seven or nine YES-NO criteria are assessed. The questions investigate the background seismicity, the uniqueness of the occurrence at the given position, the closeness to the field activity and activity period, the correlation between seismicity and withdrawal, and the possible physical mechanism. If more than half of the questions are answered by YES, the event is considered to be likely induced. Although such a discrimination approach is still qualitative, it already involves a kind of Bayesian approach to combine expert opinions and different aspects of the complex problem.

However, such weak definitions and weak regulations may be handable if enough human-related seismicity occurred in otherwise nontectonic regions with nearly no seismicity, as, e.g., North Germany, so that clear statistical correlations can be assessed. More difficult discrimination problems may arise if the geotechnical operations are situated in tectonically active regions. There, earthquakes of tectonic origin may have similar epicenters than those caused by human influence, and the YES-NO questions may not be sufficient to adequately handle the problem. The Po Plain and the Adriatic sedimentary basin in Northern Italy may be an example, among others, where oil and gas fields have been exploited in a region where natural tectonic earthquakes have frequently occurred.

The discrimination problem is even more difficult if human-triggered and human-induced earthquakes are distinguished (for definitions, see *McGarr* [1991], *Bossu* [1996], *McGarr and Simpson* [1997], *Gupta* [2002], *Dahm et al.* [2013], *Cesca et al.* [2013b, 2014], and *Shapiro et al.* [2013]). We use a definition for triggered and induced events similar to *McGarr and Simpson* [1997] and *Shapiro et al.* [2013] but further specified in terms of geometrical considerations [see also *Dahm et al.*, 2013]. According to *McGarr and Simpson* [1997], induced earthquakes are commonly understood as events where most of the stress change released during rupture was produced by the human action, while triggered events release a substantial amount of tectonic stress. *McGarr and Simpson* [1997] also point out the general motivation for such a distinction: triggered events often have a different frequency magnitude distribution and a different hazard in comparison to induced ones. Only for some few types of human actions, as, e.g., pure injection, the distinction is possibly not needed since all events are always triggered and not induced [*Gupta*, 2002; *Ellsworth*, 2013].

Recently, probabilistic discrimination criteria have been suggested in order to develop clear, quantitative, and testable discrimination rules [e.g., *Cesca et al.*, 2013a; *Dahm et al.*, 2013; *Passarelli et al.*, 2013]. Our contribution refers to this line of research and develops a probabilistic discrimination scheme for the problem of conventional production of oil and gas fields and depletion-induced and depletion-triggered earthquakes. The method is based on physical-statistical seismicity models. It considers the uncertainty in earthquake location and other input parameters and distinguishes between natural, human-triggered, and human-induced earthquakes. The method is demonstrated and tested for three examples: (1) the 2001 M_W 4.3 Ekofisk, North Sea, oil field-induced earthquake; (2) the 2004 M_W 4.4 Rotenburg, Northern Germany; and (3) the 2012 M_W 6.1 Emilia, Northern Italy, gas field-related earthquakes (Figure 1).

2. Method

We assume that an earthquake occurred near an oil or gas field that continuously produced over a period of several years and is depleted. The purpose of the scheme is to evaluate (estimate) the probability that the earthquake has been human triggered or has been human induced. We use a definition of "triggered" and "induced" suggested by *Dahm et al.* [2010, 2013] and similar to *McGarr and Simpson* [1997] but specifying—for reasons given below—the portion of large stress release on the rupture plane, instead of using an integral value only. Such a definition is similar to the one by *Shapiro et al.* [2013]. Triggered

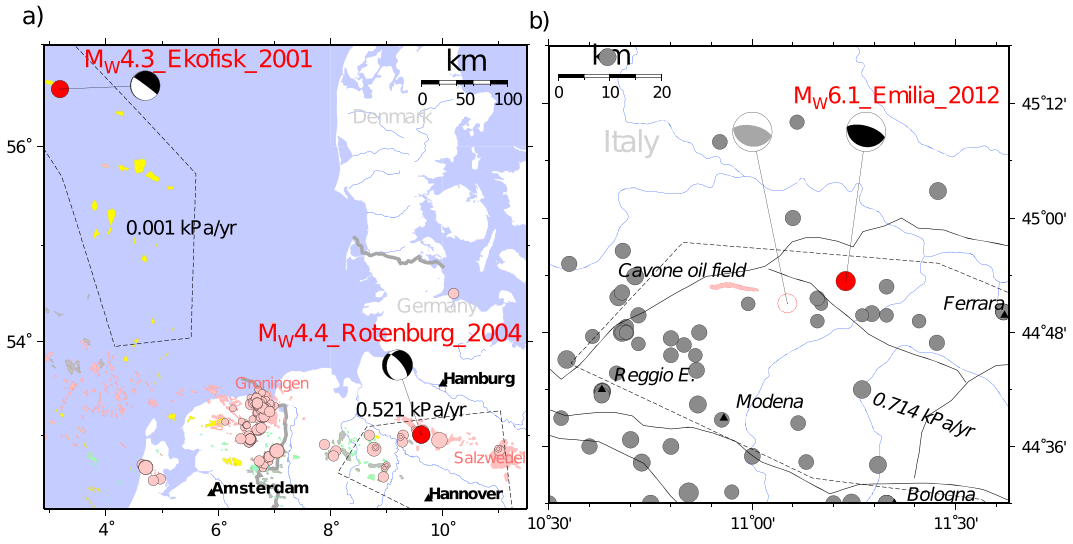

Figure 1. Overview plot. Earthquakes under study are declared as red filled circles. Dashed polygons indicate seismogenic zones [see *Grünthal et al.*, 2010; *Bungum et al.*, 2000; *Giardini et al.*, 2013]. Grey filled circles (size scaled by magnitude) indicate tectonic earthquakes prior to the studied events ($M_W > 4.5$ from 1000 to 2006, European-Mediterranean Earthquake catalogue [see *Grünthal and Wahlström*, 2012]). (a) The North Sea and Northern Germany area. Gas and oil fields are indicated by colored filled polygons (grey = Carbon, red = Rotliegend, green = Zechstein, yellow = post-Zechstein). Human-related earthquakes (1986–2012, $M > 3$) close to fields are plotted by light red filled circles (catalogues provided by BGR Hannover, Germany, and the Royal Netherlands Meteorological Institute, De Built, Netherlands). (b) The Northern Italy area. The Cavone oil field is indicated by the colored polygon. The dashed line depicts the area of the zone ITAS 293.

is understood in the sense that the rupture initiation was caused by the depletion-induced stress rate at the hypocenter of the earthquake. Rupture initiation is tested by studying the "human influence" at the hypocenter. An induced earthquake is understood in the sense that the rupture was driven by the depletion-induced stress over the full rupture plane, which, for instance, for a M_W 6 crustal earthquake may easily reach a dimension of about 10 km × 10 km [e.g., *Wells and Coppersmith*, 1994; *Blaser et al.*, 2010].

We further assume that a seismological study had been performed "a priori" and that both the hypocenter or centroid location including its uncertainty (e.g., 1σ error ellipsoid) and the source mechanism of the earthquake are known. If possible, also the fault and auxiliary plane and its respective uncertainties should have been identified a priori.

We specifically assume two periods of steady state conditions within a rock volume with linear dimension significantly larger than the rupture plane. The reference period is before the production has started, where a constant tectonic stress rate $\dot{\tau}^T$ is acting on the fault plane of the studied earthquake in rake direction of the moment tensor solution (e.g., defined as Coulomb stress rate). The background stress is related to a constant rate of earthquakes (background event rate), r^T, e.g., expressed by the rate and state seismicity model by *Dieterich* [1994]. The value r^T is defined for a given magnitude (interval). It can be estimated from the number of (similar) tectonic events per unit area and time interval. *Kostrov* [1974] established a linear relation between $\dot{\tau}^T$ and r^T by exploiting $\dot{\tau}^T \sim \langle M_0 \rangle r^T / V$, where $\langle M_0 \rangle$ is the scalar value of summed seismic moment tensors divided by the number of earthquakes and V the seismogenic volume [*Catalli et al.*, 2008; *Hainzl et al.*, 2010]. Assuming that the focal mechanisms are similar, $\langle M_0 \rangle$ can be estimated by integration of the product of the scalar seismic moment and the probability density for a given magnitude distribution. Here we assume a doubly truncated Gutenberg-Richter distribution. Then having the information of annual earthquake rate 10^a of $M \geq 0$ events (i.e., the a value), the b value, the maximum magnitude $M_{\max}$, and the area of the seismogenic zone A as well as the seismogenic width D, the background shear stress rate $\dot{\sigma}_S^T$ is [e.g., *Hainzl et al.*, 2010]

$$\dot{\sigma}_S^T = \langle M_0 \rangle \frac{10^{a-bM_{\min}}}{A\,D} = 10^{a+9.1} \frac{b}{1.5-b} \frac{10^{(1.5-b)M_{\max}} - 10^{(1.5-b)M_{\min}}}{1 - 10^{-b(M_{\max}-M_{\min})}} \frac{1}{A\,D}$$

$$\lim_{M_{\min} \to -\infty} \dot{\sigma}_S^T = 10^{a+9.1} \frac{b}{1.5-b} \frac{10^{(1.5-b)M_{\max}}}{A\,D} \qquad (b < 1.5) \tag{1}$$

Table 1. Parameter Definitions and Nomenclature[a]

Parameter	Description
$p_e(\mathbf{x})$ and $p(\boldsymbol{\theta})$	probability density distribution of the earthquake location and the model input parameter, respectively
$r(\mathbf{x},\boldsymbol{\theta})$, $r^T(\mathbf{x},\boldsymbol{\theta})$, and $r^D(\mathbf{x},\boldsymbol{\theta})$	earthquake rate: total, tectonic background, and depletion induced, respectively
$\dot{\tau}(\mathbf{x},\boldsymbol{\theta})$, $\dot{\tau}^T(\mathbf{x},\boldsymbol{\theta})$, and $\dot{\tau}^D(\mathbf{x},\boldsymbol{\theta})$	Coulomb stress rates on the fault plane in direction of observed slip: total, tectonic background, and field depletion, respectively
$p^D(\mathbf{x},\boldsymbol{\theta})$ and $p^T(\mathbf{x},\boldsymbol{\theta})$	trigger potential of being caused by field depletion or tectonic stressing, respectively
P_{trig} and P_{ind}	average probability that the event was depletion triggered or depletion induced, respectively

[a]All rate and event numbers are defined per unit volume for a given magnitude interval, $M \geq M_c$.

with units (Pa/y) if A and D are given in units of m^2 and m, respectively. The tectonic Coulomb stress rate employed is then

$$\dot{\tau}^T = \dot{\sigma}_S^T + \mu\left(\dot{\sigma}_N^T - \dot{P}_f\right) = \left[\hat{\mathbf{n}} \times \left(\mathbf{T} \times \hat{\mathbf{n}}\right) \cdot \boldsymbol{\Delta}\hat{\mathbf{u}}\right] + \mu\left(\mathbf{T} \cdot \hat{\mathbf{n}} - \dot{P}_f\right), \tag{2}$$

where $T_i = \sigma_{ij}\hat{n}_j$, $\boldsymbol{\sigma}$ is the regional stress tensor and $\hat{\mathbf{n}}$ and $\boldsymbol{\Delta}\hat{\mathbf{u}}$ are the normal and slip unit vectors of the rupture plane, respectively, P_f is the pore pressure in the rock and μ is the friction angle in the Coulomb failure law.

If the tectonic surface displacement field has been accurately measured, and the coupling of the plate is sufficiently well known, $\dot{\tau}^T$ may alternatively be estimated from strain rates.

The second period under consideration is defined some years after the start of oil or gas recovery until the occurrence of the event. Most often, the annual production rates are roughly constant after the infrastructures are installed. We use a constant depletion rate for simplicity. If $\dot{\tau}^D$ is the depletion-induced Coulomb stress rate on the fault, the total acting stress rate is $\dot{\tau} = \dot{\tau}^T + \dot{\tau}^D$. Accordingly, the expected total earthquake rate in the volume under consideration is $r = r^T + r^D$. Usually, r^T is a smooth function of space, while r^D and $\dot{\tau}^D$ are variable functions of space, decaying to zero if the fault is far from the exploited field. Employing the Dieterich seismicity model [e.g., *Dieterich*, 1994, 1995] under steady state conditions, it is easy to show that

$$\frac{r}{r^T} = \frac{\dot{\tau}}{\dot{\tau}^T} \text{ and accordingly } \frac{r^D}{r^T} = \frac{\dot{\tau}^D}{\dot{\tau}^T}. \tag{3}$$

We will use this relation together with (2) to derive r^D and r and to define a trigger probability. For instance, the depletion-induced stress rate can be estimated by elastic modeling considering the concept of nuclei of strain [e.g., *Geertsma*, 1973]. Since we do not want to evaluate the effect of possible stress shadows, we will consider only values of $\dot{\tau}^D \geq 0$ and therefore define the human-induced stress rate by $\dot{\tau}^D H(\dot{\tau}^D)$, where H defines the Heaviside function. In other words, we will discard here the possible stabilizing effect of field depletion on earthquake occurrence, where P_{trig} is a priori zero.

The probabilistic discriminatory method is straightforward. An overview of the parameter definitions and nomenclature is provided in Table 1. The set of model parameters to calculate $\dot{\tau}^D/\dot{\tau}^T$ is mapped into vector $\boldsymbol{\theta}$. We first define a trigger potential that an event, which was located at point $\mathbf{x}$, has been triggered by depletion

$$p^D(\mathbf{x},\boldsymbol{\theta})) = \frac{r^D(\mathbf{x},\boldsymbol{\theta})}{r^D(\mathbf{x},\boldsymbol{\theta}) + r^T(\mathbf{x},\boldsymbol{\theta})} = \frac{H(\dot{\tau}^D)\dot{\tau}^D(\mathbf{x},\boldsymbol{\theta})}{H(\dot{\tau}^D)\dot{\tau}^D(\mathbf{x},\boldsymbol{\theta}) + \dot{\tau}^T(\mathbf{x},\boldsymbol{\theta})}. \tag{4}$$

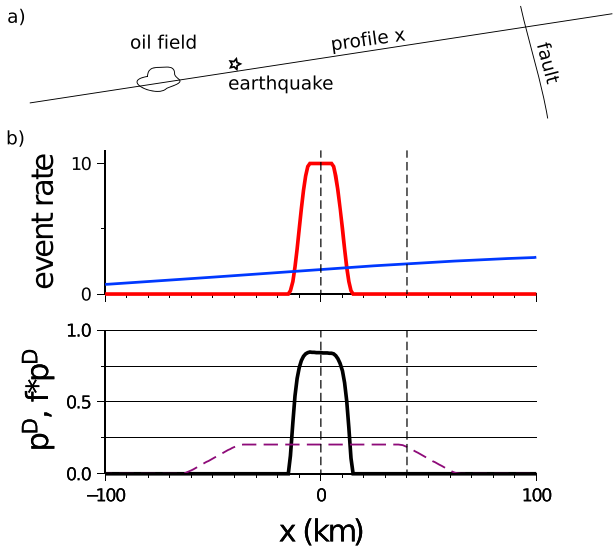

Figure 2. Sketch to illustrate the approach in 1-D. (a) Geometry of the problem. An earthquake is located close to an oil field and in some distance to an active tectonic fault. (b) The depletion-induced (red) and tectonic event rates (blue) are plotted along profile x, where the oil field is situated between −10 km and 10 km. Below, the trigger potential p^D (black solid line) is plotted together with the filtered function $f * p^D$ (dashed), where the filter length of the boxcar function was 100 km. Vertical dashed lines specify the centroid positions of two hypothetical earthquake centroids.

This function gives the probability that the rupture nucleation was triggered by field depletion assuming that we know exactly the hypocenter location of the earthquake (Figure 2, black solid line). The trigger potential, assuming that the event was of tectonic cause, p^T, is similarly equated by replacing r^D by r^T in the denominator so that $p^T(\mathbf{x},\theta) = 1 - p^D(\mathbf{x},\theta)$. Note that the same approach (equation (4)) is used to calculate the probability to be an aftershock or background event [*Zhuang and Ogata*, 2004].

In practice, spatial coordinates and parameter values are discretized on regular grids, and we may calculate p^D at each grid point in a volume under study. The trigger potential has to be considered at the hypocenter of the earthquake. If we would not know where the earthquake occurred, the maximum of p^D would indicate the most likely location and parameter value given that the event was depletion triggered, while the maximum of p^T would indicate the most likely location given that the event was tectonic triggered.

The hypocenter location uncertainty can be given in terms of the probability density function (pdf) $p_e(\mathbf{x})$. For instance, well-located earthquakes may have a Gaussian location likelihood as $p_e(\mathbf{x}) = \frac{1}{[2\pi]^{3/2}s_x s_y s_z} e^{-\frac{1}{2}\frac{(x-\bar{x})^2}{s_x^2}} e^{-\frac{1}{2}\frac{(y-\bar{y})^2}{s_y^2}} e^{-\frac{1}{2}\frac{(z-\bar{z})^2}{s_z^2}}$, where $(\bar{x},\bar{y},\bar{z})$ declares the best hypocenter location and (s_x, s_y, s_z) the 1σ standard deviation. If the uncertainty of the location is large, p_e may be a flat constant likelihood over some distance with radius r. For instance, r may be defined from macroseismic data and then used to define a volume V to suggest an equal distribution location likelihood as $p_e = 1/V$ (or $p_e = 1/A$ for an area approach). If we consider the location pdf and equivalently the pdf of the input parameter, $p(\theta)$, the trigger probability can be equated by

$$P_{\text{trig}} = \int_V \int_\theta p^D(\mathbf{x},\theta)\, p_e(\mathbf{x})\, p(\theta) \mathrm{d}\theta \mathrm{d}\mathbf{x}\,. \tag{5}$$

If uncertainties are present, P_{trig} is the weighted average of the trigger potential from the values sampled by the pdfs of the input parameter and the hypocenter location (Figure 2). We calculate the probability by a bootstrapping approach: locations and parameters are randomly sampled from their pdfs, and the resulting distribution of the trigger potential is analyzed in terms of its average or median and its spread in terms of a standard deviation or percentile.

Equation (5) is used to estimate the trigger probability of the hypocenter of the event, i.e., the nucleation point of rupture. This corresponds to the probability that the earthquake was triggered by field depletion, independent of the question whether a large portion of the rupture was driven by tectonic stress or not and whether a large portion of the rupture plane lies outside the volume influenced by field depletion. If we want to test whether the complete rupture was likely driven by depletion-induced stress rates, we calculate the average trigger probability of all possible nucleation points on the rupture plane, independent of the question where the true nucleation point was. If the earthquake rupture is viewed as a subsequent triggering of many small rupture segments, each single rupture segment would have had, on average, a high likelihood of being human triggered. Although this simplified model is only a rough approximation of a physical rupture, i.e., since segment-segment interaction is neglected, it can be used as a proxy for

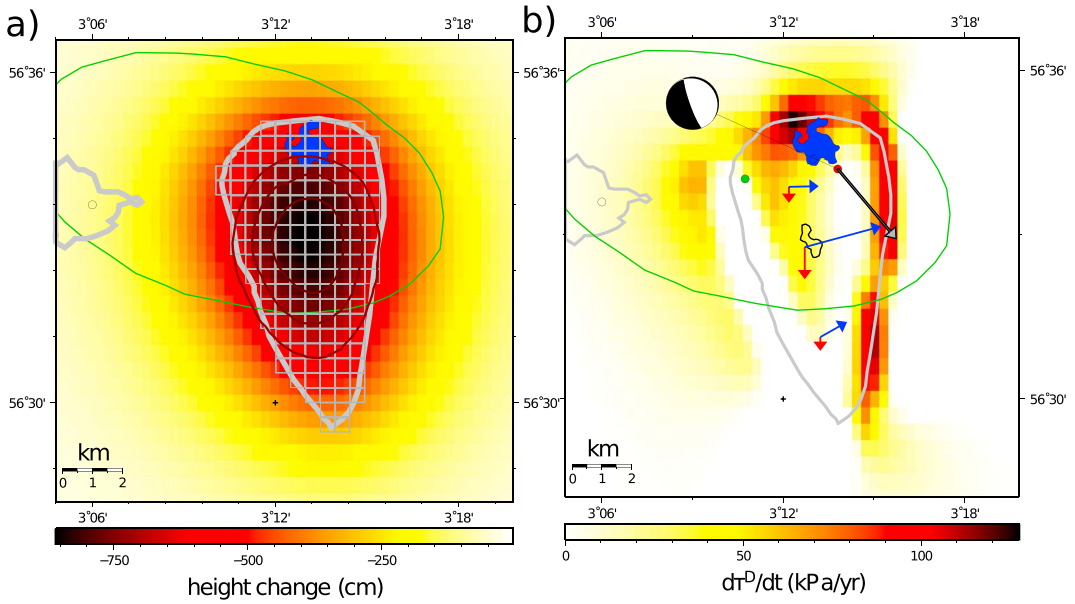

Figure 3. Stress and location model for the Ekofisk case. The green line indicates the error ellipse derived from travel-time inversion. The Ekofisk and West Ekofisk oil fields are indicated by thick grey lines. The blue filled polygons show an area of localized preseismic uplift due to unintended water injection [see *Ottemöller et al.*, 2005]. (a) Comparison of measured (colored contours) and modeled subsidence bowl (colored grid) in 2001 by simulating nuclei of strain at 3 km depth at the given rectangular boundary elements.(b) Simulated Coulomb stress rate (colored grid) on a subhorizontal plane in 2 km depth parallel to the assumed fault plane. The source mechanism of the earthquake is indicated by lower hemispherical projection of the *P* wave radiation pattern. The thick black arrow indicates the centroid location and rupture direction as derived from the kinematic waveform inversion [*Cesca et al.*, 2011]. The blue and red arrows show the GPS-observed near-field coseismic ground motion in horizontal and vertical direction, respectively. The black cross is a reference point.

the discrimination between triggered and induced earthquakes. The test may be realized by defining a representative volume embedding the rupture plane. This is either retrieved from a seismological kinematic source inversion or by means of scaling relations. For instance, the volume may be formed by the rupture plane with length L and width W as base and one grid size in perpendicular height. If the location of the rupture plane is not well constrained, the perpendicular height may be increased or a cube around the centroid may be chosen if the rupture plane orientation is uncertain. Then, each centroid point $\mathbf{x_i}$ in p^D has to be integrated in each coordinate direction over the length interval defined by the chosen volume, e.g., in length direction along strike in the interval $[x_i - L/2, x_i + L/2]$. The integration represents a smoothing operation, e.g., a convolution with a fault-like boxcar function (fault filter). For the test of an induced earthquake, we therefore first smooth the trigger potential with a fault filter $f(\mathbf{x_i}, L, W, \text{strike}, \text{dip})$ and apply then equation (5) to the filtered results of $f * p^D$

$$P_{\text{ind}} = \int_V \int_\theta \left[f(\mathbf{x}, L) * p^D(\mathbf{x}, \theta) \right] p_e(\mathbf{x})\, p(\theta) \mathrm{d}\theta \mathrm{d}\mathbf{x}\,, \tag{6}$$

where $*$ declares a convolution integral. The fault filter is normalized so that its integral is equal to 1. Equation (5) can be interpreted as a special case of (6) for which the length L is reduced to the grid size of the centroid points under testing.

P_{ind} is usually smaller than P_{trig}. This is illustrated in Figure 2. For instance, the earthquake under study may have had a magnitude of M 7 and a fault size of 10 km × 100 km. The dimension of the stress rate anomaly of the oil field is possibly only 20 km in diameter. If the earthquake nucleated in a distance of 40 km from the center of the oil field, the trigger probability in our case would be zero. If it nucleated directly above the field, the trigger probability in our example would be nearly 80%. However, the probability to be induced over the fault length of 100 km is less than 20% even above the field (Figure 2, dashed curve), so P_{ind} will be small even if location uncertainties would be taken into account. The nucleation of the hypothetic M 7 earthquake would have been human triggered, but the 100 km long rupture would be classified to be

not human related and mostly driven by tectonic stress. This is in line with interpretations given by others [e.g., *McGarr and Simpson*, 1997].

3. Applications

3.1. The 2001 M_W 4.3 Ekofisk, North Sea, Earthquake

The 7 May 2001 M_W 4.3 Ekofisk induced earthquake was located in close proximity to the Ekofisk oil fields in the North Sea with a water depth of about 80 m (Figure 3a and, e.g., *Ottemöller et al.* [2005]). The Ekofisk oil field is situated in about 3.1 km depth within the post-Zechstein formation below an overburden mostly composed of clay and shales, interbedded by silty streaks [*Abdulraheem et al.*, 1994]. The earthquake location uncertainties were 4.7 km in latitude and 7.6 km in longitude [*Ottemöller et al.*, 2005]. A detailed waveform modeling combining broadband regional and teleseismic data with near-field Global Positioning System (GPS) data retrieved a best focal mechanism with strike 161°, dip 77°, rake −100°, scalar moment $2.85 \cdot 10^{15}$ Nm, and depth of 2 km. Especially the near-field GPS data with observed uplift could demonstrate, in combination with the retrieved source mechanism, that the seismic source centroid was shallow above the field formation at the eastern border of the field [*Cesca et al.*, 2011]. A kinematic inversion for parameters of the extended source and rupture further indicated that the subhorizontal plane ruptured unilaterally over a length of about 6 km in azimuthal direction of about 133° [*Cesca et al.*, 2011]. The kinematic solution further indicated a very slow rupture velocity of only about 500 m s^{-1} (equal to 0.26 times the shear wave velocity) and a long rise time of about 7 s. The unusual slow and long rupture explains that such a moderate-strong earthquake was able to radiate energetic low-frequency Rayleigh and Love waves well observed up to 2000 km epicentral distance. As suggested by *Ottemöller et al.* [2005] and supported by the kinematic source inversion of *Cesca et al.* [2011], the rupture was likely to be triggered by an unintended water injection during about 2 years of $1.9 \cdot 10^6$ m^3 in 2 km depth near the northern central part of the field [*Ottemöller et al.*, 2005] (see Figure 3a for location). The triggering of the earthquake rupture may have been realized by the formation and slow growth of a large horizontal hydrofracture within the overburden in about 2 km depth within the shale and mud rocks. The creation and subhorizontal orientation of such a hydrofracture was likely during the period of the water leakage because of the high injection pressure exceeding the tensile strength of the sediments [see *Ottemöller et al.*, 2005, Figure 11] and because of the shape of the depletion-induced stress ellipsoid was favorable for horizontal fracture growth. The uplift retrieved by differential bathymetry before and after the earthquake in the region of the water injection hole [see *Ottemöller et al.*, 2005] supports the idea that a subhorizontal hydrofracture did form.

Knowing the earthquake hypocenter and centroid location, the rake direction and the size and depth of the fault plane, we aim to test whether the earthquake was natural, depletion triggered, or depletion induced.

A first step is to derive a depletion-induced stress rate model for the volume of the overburden above the oil-bearing layer. As a consequence of the pore pressure decrease in the reservoir, the reservoir formation compacts and the rock volume above and below the reservoir deforms. We use the model of nuclei of strain [*Geertsma*, 1973] and simulate the depletion effect considering the extent, shape, and depth of the Ekofisk oil field. The oil field is approximated as a thin porous layer embedded in an impermeable half-space. We assume a half-space model with a shear modulus of 6 GPa and a Poisson ratio of 0.25. Note that the absolute values of the elastic modules are not very important, since we calibrate the stress and pore pressure model by the measured seafloor subsidence. For instance, assuming a stiffer overburden predicts larger pore pressure reductions to explain a given subsidence rate (deformation) but leads to similar stress rates in the rock.

Field geometry is often irregular and of large extent, and 3-D modeling is needed to analyze the problem. We modify a 3-D displacement discontinuity method to consider the effect of undrained poroelastic field depletion. The thickness, Biot's constant, and effective uniaxial compaction coefficient of the field are considered (Appendix B).

The maximal value of the depletion-induced subsidence of the seafloor over a production period of about 30 years occurred roughly in the middle of the Ekofisk field and was more than 8.26 m (Figure 3a). The Ekofisk field is neither circular nor disk shaped, and our simulated subsidence pattern is therefore not exactly bowl shaped as predicted by analytical solutions [e.g., *Geertsma*, 1973; *Chan*, 2004]. Our reservoir pore pressure model explains well the general pattern and quantitative values of the subsidence in terms of magnitude and shape (Figure 3a). A pore pressure decrease of about 47 MPa is needed to explain the

Table 2. Seismicity Parameters (Taken From SHARE Project [*Giardini et al.*, 2013]) and the Resulting Tectonic Stress Rate From Equation (1) With Its Standard Deviation (in Brackets)[a]

Earthquake	Source Zone	A (km^2)	a	N ($M \geq 5$/year)	b	M_{max} (Weight)	D (km)	$\dot{\tau}^T$ (Pa/yr)
Ekofisk	NLAS037	174,800	2.8	0.006	1.0	6.5 (0.5), 6.7 (0.2), 6.9 (0.2), 7.1 (0.1)	20	1.1 (0.4)
Rotenburg	BAAS191	39,800	3.7	0.158	0.9	7.3 (0.5), 7.5 (0.2), 7.7 (0.2), 7.9 (0.1)	16.0	521.7 (274.5)
Emilia	ITAS293	11,080	3.7	0.050	1.0	7.3 (0.5), 7.5 (0.2), 7.7 (0.2), 7.9 (0.1)	10.0	714.7 (388.0)

[a]Details of the determination of the seismicity parameters can be found at http://www.share-eu.org. Uncertainties are taken into account by (i) probabilities for M_{max} as provided by SHARE (see table), (ii) uniform distributed rates N ($M \geq 5$/year) within ±50%, (iii) uniform distributed b values with $b \pm 0.1$, and (iv) uniform distributed D values within $D \pm 5$ km the corresponding distribution of a values is calculated by $a = \log(N) + 5b$. The scale factor of $w = 1$ is assumed in (2) since the earthquakes were favorable oriented with respect to the regional stress orientation.

subsidence over the period of 30 years. If we assume a homogeneous production rate, this results in a pore pressure reduction rate of about 1.6 MPa/yr. This estimate is well in agreement with an initial pore pressure in the Ekofisk field of about 47 MPa, dropped to nearly zero during the production period [*Ottemöller et al.*, 2005] and supports the choice of parameter in the modeling study.

From the reservoir depletion model we calculate the stress rate for each stress component at each half-space grid point with a spacing of 500 m. Figure 3b shows the Coulomb stress rate in direction of the slip vector of the earthquake on a horizontal plane at 2 km depth. It is noteworthy that the highest Coulomb stress rates up to 120 kPa/yr occur along the northern and eastern borders of the field where the rupture was located by *Cesca et al.* [2011]. The Coulomb stress rate in Figure 3b is associated with $\dot{\tau}^D$, a parameter needed in the discriminatory equation (5).

The other quantity needed is the natural stress rate $\dot{\tau}^T$. The Ekofisk oil field is located within the North Sea Central graben system, a failed continental rift system that was formed during the Triassic and Jurassic periods and is inactive today. The historical and instrumental seismicity over the last 100 years is minor. The Viking graben, which is north of the Central graben, appears slightly more active than the Central graben system [e.g., *Bungum et al.*, 1991]. The largest instrumentally recorded earthquake in the North Sea was the M_L6.1 1931 Dogger Bank earthquake off coast SE England. However, this is about 300 km south of Ekofisk and not associated with the seismic zone of Central graben at Ekofisk. The average recurrence period for $M > 3.8$ in the seismic zone of the Ekofisk event is about 100 years, with a b value of about 1 [*Bungum et al.*, 2000; *Grünthal et al.*, 2010; *Giardini et al.*, 2013]. The average tectonic stress rate is estimated $\tau^T \approx (1.1 \pm 0.4)$ Pa/yr (5% and 95% percentiles at 0.5 Pa/yr and 2.0 Pa/yr, respectively) depending on the assumed seismogenic thickness and maximal magnitude M_{max}. The estimates in Table 2 are considered to contain the minimal and maximal bounds of the tectonic stress rate. The estimated upper limit is possibly too high. For comparison, the tectonic stress rate in the Central Appennines graben system in the region of Aquila, where several $M < 6$ earthquakes were reported during historical times, is estimated at about 0.7 kPa/yr [*Catalli et al.*, 2008].

Figure 4 shows the result of the discrimination tests by using an upper bound value of $\dot{\tau}^T = 0.0015$ kPa/yr and a pore pressure drop in the oil field of $\Delta P \approx 47$ MPa (5% and 95% percentiles at 44 MPa and 50 MPa, respectively). Figure 4a shows the discrimination trigger potential p^D in a plane at 2 km depth. Over the region of the location uncertainty, p^D is almost always close to 1. The estimated probability that the Ekofisk earthquake has been triggered by field depletion is close to 0.99.

We test whether the Ekofisk event was not only triggered at the nucleation point but depletion driven over the full size of its rupture plane. Figure 4b shows the probability to have been induced if we filter p^D with fault filter of 10 × 10 km so that the fault would cover nearly half of the area of the Ekofisk field. The trigger potential function is therefore spatially smoothed. The probability to be induced is estimated still very high at $P_{ind} \approx 0.74 \pm 0.28$.

3.2. The 2004 M_W 4.4 Rotenburg, Northern Germany, Earthquake

The 20 October 2004 M_W 4.4 Rotenburg earthquake occurred in close proximity to the three most productive gas fields in North Germany, the Söhlingen, the Rotenburg, and the Völkersen fields (Figure 5a). Three aftershocks with M_L between 1.7 and 2.2 could be detected and located during the first 4 days after the main shock. The events were in proximity to the southwestern border of the Söhlingen field, which is situated in the Rotliegend Dethlingen sandstone in 5.8 km depth. The tight gas field is covered by Zechstein

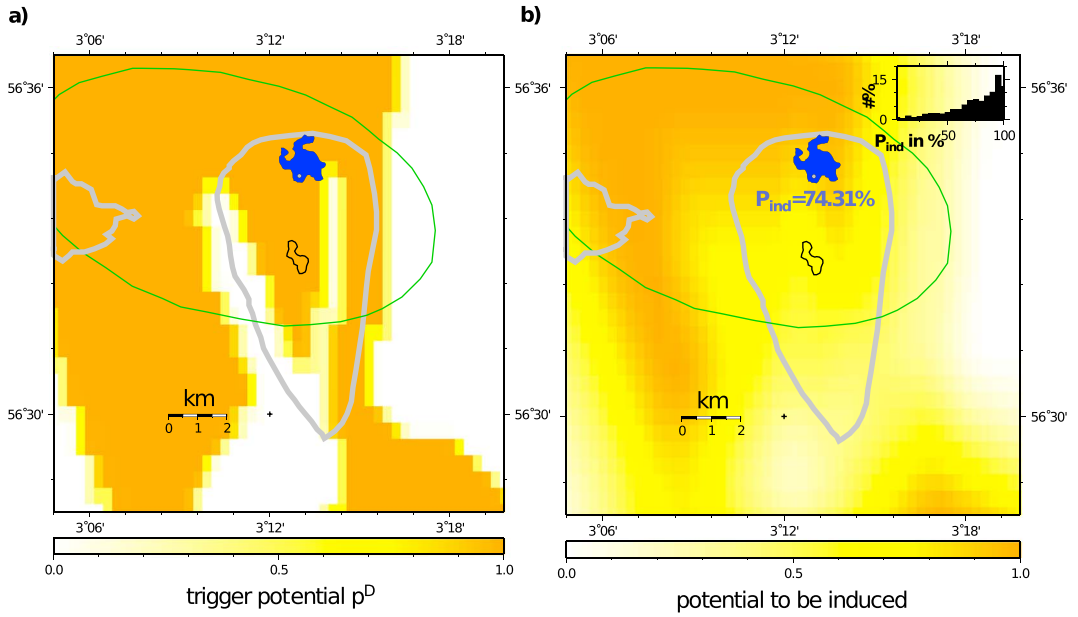

Figure 4. (a) The trigger potential at 2 km depth from depletion of the Ekofisk oil field (colored grid) is plotted together with the location error ellipse (green solid line). The trigger potential was calculated for the subhorizontal plane. Oil platforms are indicated. (b) Same as in Figure 4a but for the potential that the M_W 4.3 earthquake was induced assuming a fault filter dimension of 5 × 5 km. The inlet figure shows the frequency distribution of the induced probability.

salt, which formed at the position of the Söhlingen field a salt dome. The subsalt Rotliegend layer is cut by several NNW-SSE striking, deep angle normal faults with offsets of about 100–200 m (e.g., Geotectonic Atlas [*Baldschuh et al.*, 2001] and from published geological cross sections at drilling site of Z16 borehole in 2006). A detailed seismological study [e.g., *Dahm et al.*, 2007] revealed an epicentral location at 9.625° longitude and 53.009° latitude with an error ellipse of 7.3 km and 5.8 km half-length of the principal axis (inclined by azimuth of 100°). The hypocentral depth was estimated between 5.0 and 6.4 km from teleseismic depth phases at seismological arrays in USA and Canada [*Dahm et al.*, 2007]. In the present study we use a depth at (6 ± 5) km. The retrieved seismic moment was M_W 4.4, the rupture duration 1.32 ± 0.6 s, and the rupture

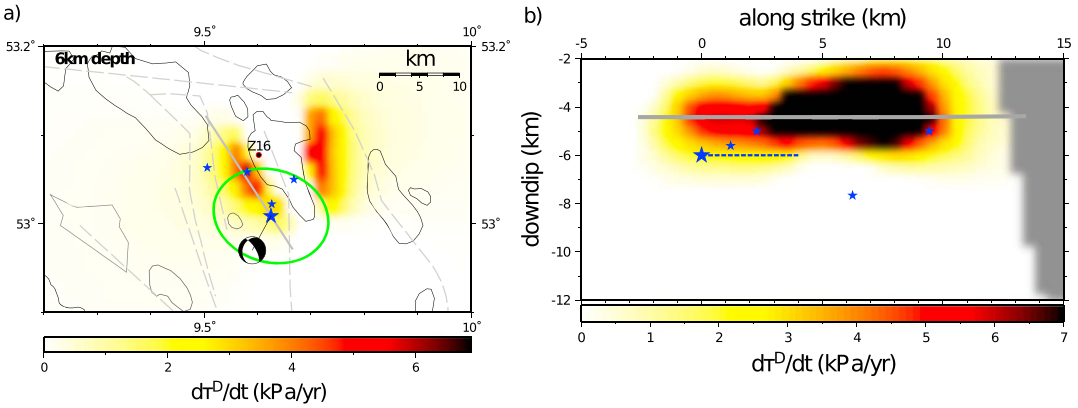

Figure 5. Coulomb stress rate models (colored grid) are plotted together with the location of the main shock and three aftershocks of the Rotenburg sequence (blue stars). (a) The green line indicates the epicenter error ellipse derived from traveltime inversion. The Söhlingen gas field and other neighboring gas fields are indicated by grey polygons. The moment tensor source mechanism is given by lower hemispherical projection (see *Dahm et al.* [2007] for details). Coulomb stress rate was calculated on a horizontal grid in 6 km depth in earthquake slip direction for planes subparallel to the NE dipping fault plane. Dashed grey lines indicate mapped basement faults in about 6 km depth from the Tertiary period [*Brückner-Röhling et al.*, 2004]. Z16 shows the position of a fracking borehole drilled in 2006 (see text for further explanation). (b) Coulomb stress rate is plotted on a grid along strike and downdip on the assumed fault plane (see grey solid profile in Figure 5a). The projected depth of the Söhlingen field is indicated by the thick grey line.

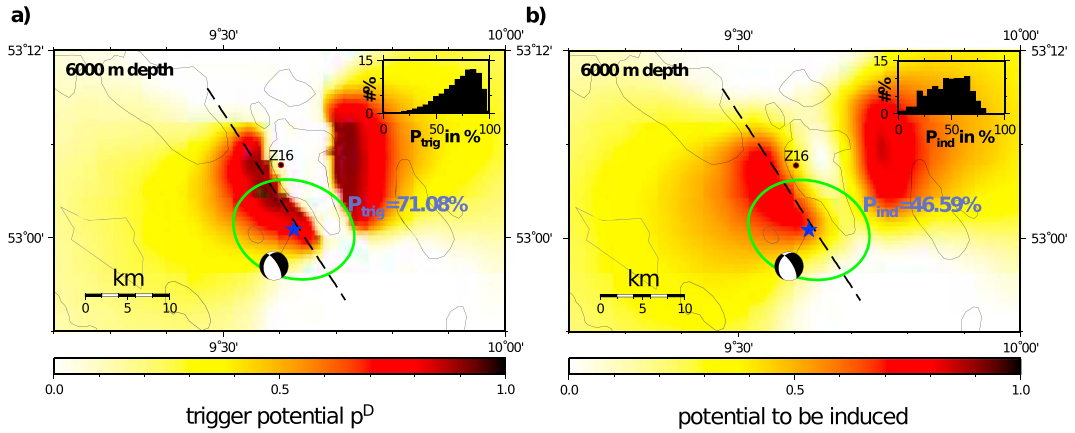

Figure 6. (a) The trigger potential at 6 km depth from depletion of the Söhlingen gas field (colored grid) is plotted together with the location (blackfilled circle, location uncertainties in green) and source mechanism of the Rotenburg M_W4.4 earthquake. The trigger potential for normal faulting mechanism is outside the border of the gas field. The inlet figures show the frequency distribution of P_{trig} at the epicenter. The bootstrapping of uncertainties have been realized by avoiding the stress shadow directly beneath the gas field. (b) Colored grid shows the potential that M_W4.4 earthquakes with the mechanism of the Rotenburg event are induced assuming a fault filter dimension of $5 \times 5 \times 5$ km. The inlet figures show the frequency distribution of the induced probability.

length 4.6 $\pm$ 2 km with indication of an unilateral rupture in northward direction. The inverted normal faulting source mechanism with strike 327°, dip 72°, and rake −117° (Figure 5a) agrees well with the indicated strike and dip of sub-Zechstein faults at the western border of the Söhlingen field.

The Rotenburg/Söhlingen region is considered of moderate seismicity. It bears one of the smallest seismic hazards in Germany. The Rotenburg earthquake was the strongest event ever recorded in Northern Germany, if other human-induced events are discarded. However, a moderate earthquake with M_L 4 occurred in 1977 about 20 km SE to the Rotenburg earthquake. Although this event occurred in the belt of gas fields in the Rotliegend formation and although its reverse source mechanism and orientation is not typical for the regional stress, it was at the time of occurrence not associated to gas production.

The tectonic stress rate in the seismic zone of the Rotenburg events is estimated in between $\dot{\tau}^T = (0.5 \pm 0.27)$ kPa/yr (5% percentile and 95% percentile at 0.2 kPa/yr and 1 kPa/yr, respectively) depending on the assumed seismogenic thickness, b value, and maximal magnitude M_{max} (see Table 2 for specific values).

Figure 5 shows our estimated Coulomb stress rate from depletion of the Söhlingen field. A depletion-related pore pressure drop of 10 MPa was used for the figure. For the uncertainty analysis of the trigger likelihood we used 5% and 95% percentiles of ΔP at 5 MPa and 20 MPa, respectively. The maximal stress rates at 6 km depth have values slightly larger than $\dot{\tau}^D \approx 6$ kPa/yr and are found within a narrow belt at the western and eastern borders of the Söhlingen field. The depletion-induced stress rate is about a factor of 20 smaller than for Ekofisk, but still a factor of about 10 larger than the regional tectonic stress rate. The maximum of the induced stress rate anomaly aligns pretty well with the location and strike direction of the assumed sub-vertical fault plane [see *Dahm et al.*, 2007; *Cesca et al.*, 2010]. The downdip and along-strike cross section of the stress rate shows that largest rates were observed beneath the field in a depth range of 3–7 km. From the seismological study we know that the rupture initiated at the southern tip of the high-stress region and propagated toward the region of higher stresses. The pattern of the Coulomb stress rate depends mostly on the location, depth, and shape of the gas reservoirs, which are well known. The absolute values of the Coulomb stress rate, however, are more uncertain, since we could not calibrate the reservoir pore pressure model by means of observed surface subsidence, which was not available. We estimated the pore pressure reduction at field level by means of thermodynamic relations considering the published production rates (see Appendix B). However, for the analysis we use a broad range of pore pressure drops to bootstrap the uncertainties.

Figure 6a shows the discrimination trigger potential together with the location error ellipse. The trigger potential in 6 km depth is high outside the eastern and western rim of the gas field, with relatively sharp boundaries. Above and below the gas field, the trigger potential is zero. This can be expected, since normal

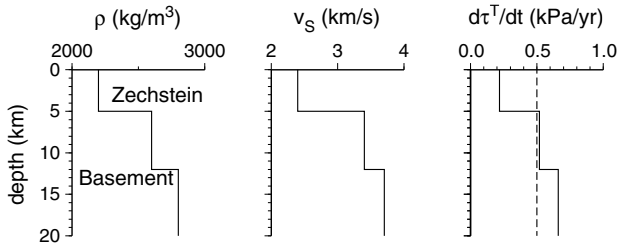

Figure 7. Depth-dependent stress rate model: density ρ, shear wave velocity v_S [e.g., *Dahm et al.*, 2007, Figure 5a], and assumed stress rate $\dot{\tau}^T$ in the sediments and upper basement of the North German basin. Stress rate scales with shear modulus $= v_S^2 \rho$, assuming $\rho_{\text{Zechstein}} \approx 2200$ kg/m^3, $\rho_{\text{SubZech}} \approx 2500$ kg/m^3, and $\rho_{\text{Basement}} \approx 2800$ kg/m^3. The average stress rate is indicated by dashed line.

faulting mechanisms as observed for the Rotenburg event are favorable oriented outside the border of a field, and above and directly beneath the field stress shadows are expected for normal faulting events. If we bootstrap the uncertainties of the input parameter and location, we retrieve a probability of $P_{\text{trig}} = 0.71 \pm 0.20$, indicating that the Rotenburg earthquake was likely triggered by field depletion-induced stresses.

The rupture length of the Rotenburg earthquake, based on waveform inversion, is about 4 km. It is only about half the length of the Ekofisk event. We define a fault filter of $5 \times 5 \times 5$ km^3 to test the hypothesis that the Rotenburg earthquake was induced by field depletion. Because of the filtering, the trigger potential function in Figure 6b is smoothed and reduced in its absolute level. The likelihood of being induced is estimated with $P_{\text{ind}} = 0.46 \pm 0.18$. Figure 6b shows also the distribution of P_{ind}. The result indicates that the Rotenburg earthquake was triggered by field depletion and with about 50% likelihood also depletion induced.

Tectonic stress rates are possibly depth dependent within the uppermost crust. For instance, shallow tectonic earthquakes (natural) are seldomly observed in the uppermost layers of the North German sedimentary basin, which may be explained by a reduced tectonic (brittle) stress rate in the basin. The North Germany sedimentary basin in the study region is about 10–12 km thick. Major density and seismic velocity interfaces exist at about 5 km depth, between the Zechstein salt and sub-Zechstein sediment layers, and at about 12 km depth at the basement of the basin. We keep the average stress rate of $\dot{\tau}^D = 0.5$ kPa/yr unchanged (see Table 2) and assume that stresses acting on each possible subfault arise from (constant) tectonic strain acting through the elastic medium and from slip of all other neighboring fault elements, in the sense of a rate and state seismicity model. Then, the stress rate at depth scales with the relative shear rigidity in the basin [see *Dieterich*, 1995, equation (1)]. Figure 7 shows the assumed variation of the stress rate with depth. The generic, depth-dependent tectonic stress rate model is possibly a better approximation to reality than a depth-independent model and explains the lack of seismicity in shallow sediments. Our main motivation for the modified model, however, is to demonstrate the ability to consider depth-dependent stress rates and how they may influence the discrimination probabilities.

Figure 8 shows p^D in vertical cross sections for depth-dependent and homogeneous stress rates (see Figure 7). The pattern of p^D is very similar in both cases and shows high probabilities to be triggered down to 8 km depth. The depth-dependent case (Figure 8a) indicates slightly higher values of p^D at shallower depth,

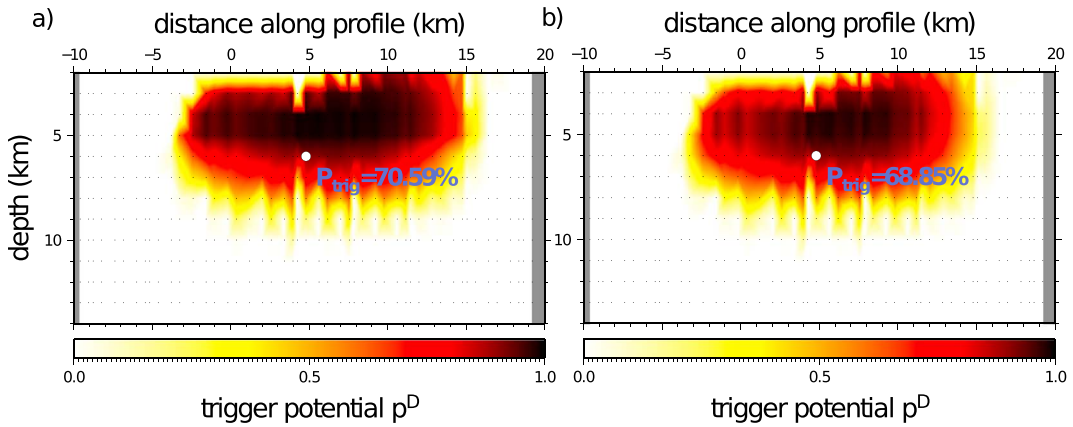

Figure 8. Trigger potential function p^D calculated on a vertical section through the profile defined in Figure 6. Results are calculated for the (a) depth-dependent and (b) depth-independent tectonic stress rate of Figure 7.

because there the tectonic stress rate was reduced. Since the bootstrap sampling of the uncertain location depth samples also the shallower regions above the hypocenter, the average trigger probability is slightly larger than the value extracted for the depth-independent case (Figure 8b). If the earthquake would have occurred at depths beneath 12 km in the granitic basement, p^D would have been relatively small indicating a natural origin of the earthquake. For instance, if we rerun the calculations assuming a hypothetical earthquake depths at (14 ± 5) km and a small depth uncertainty of ±1 km, the triggering probability is about (5 ± 8)%. This demonstrates that a well-constrained earthquake depth is helpful to evaluate the trigger questions, while depth-dependent tectonic stress rates add only relatively little to the question.

3.3. The 2012 M_W 6.1 Emilia, Northern Italy, Earthquake

On 20 May 2012 a strong earthquake of M_W 6.1 occurred in the sedimentary basin of the Po Plain in Northern Italy. The intensive sequence of aftershocks struck a relatively large area; the largest one occurred on 29 May and had a moment magnitude of M_W 5.9. Both main and largest aftershocks caused significant damage and losses. Partial structural collapses of historical buildings and industrial facilities unfortunately caused 27 fatalities and the evacuation of more than 15,000 people. The maximal intensities of the 20 May 2012 and the 29 May 2012 earthquakes were $I_0 = VIII$ (multichannel seismic). A centroid moment tensor inversion for the largest shocks of the sequence found a centroid depth between 6.2 and 8.0 km [*Cesca et al.*, 2013c]. A thrust mechanism on WNW-ESE striking planes was retrieved in accord with the orientation of the tectonic stress and with the strike of known local fault structures [e.g., *Basili et al.*, 2008]. A kinematic source inversion and directivity analysis resolved that the SSW dipping low-angle fault was activated as rupture plane over a length of about 15 km [*Cesca et al.*, 2013c]. This rupture plane could also be associated to a postulated blind thrust fault (Mirandola fault) with an assumed potential for M_W 6.3 shocks [*Basili et al.*, 2001], which has also been indicated by geomorphological structures of river anomalies [*Burrato et al.*, 2003]. Historical seismicity before 2012 indicated that the up to 8.5 km thick sedimentary Po Plain foredeep basin is affected by a diffuse pattern of seismicity up to M_c 5.6. As a consequence of the collision between the European and African plates, the Po Plain develops buried shallow thrust faults accommodating the continuous convergence. The Northern Apenninic thrust fronts, a system of several such outer arc faults, cut the region of the Emilia 2012 earthquakes. The epicentral area is associated to the compressional tectonics of the Po Plain Adriatic front, covered by the seismic zone ITAS293 [see *Giardini et al.*, 2013] for which we derive a tectonic stress rate $\dot{\tau}^T$ of 0.7 ± 0.38 kPa/yr (see Table 2). Using data from the hazard study by *Meletti et al.* [2012, zone 912] would lead to estimated stress rates of 0.13–2 kPa/yr. The stress regime is compressional.

The two largest events of the seismic sequence are located east of the so-called Cavone-Mirandola anticline. This area includes three hydrocarbon exploitation licenses, Mirandola (including the Cavone field), Spilamberto, and Recovato, as well as the gas storage reservoir Minerbio and the geothermal field of Casaglia (Ferrara) [*Styles et al.*, 2014]. The Cavone oil field is nearest to the seismic activity. We tested the possible effect of the depletion of the Cavone oil field on the occurrence of the Emilia main shock.

The production of the Cavone field started in 1980 from a 400–700 m thick anticline located between 2.5 km and about 3.2 km depth in Mesozoic carbonate rocks. [*Styles et al.*, 2014, Figures 1 and 9a]. The anticline structure is elongated about 12 km in EW direction and covers a total surface area of about 15 km^2. In 2012 a volume of about 3.06 Mm^3 of oil had been recovered. Since 1993, about 2.6 Mm^3 of produced waste water has been reinjected at the bottom of the same thick reservoir at a depth of 3.35 km so that the fluid pressure in the reservoir seems to have been nearly maintained, likely supported by additional inflow from a nearby aquifer. In the modeling study by *Styles et al.* [2014] the pore pressure in the reservoir is assumed to have dropped about 1 MPa over the lifetime of production. Measured effective injection pressure at the wellhead of the injection well was initially 18 MPa and varied between 21 MPa and 13.8 MPa. In May 2012, the injection wellhead pressure was 19 MPa. A direct hydraulic contact between the Cavone reservoir and the seismogenic thrust zone is not indicated, because of several highly impermeable layers in the stratigraphic sequence [e.g., *Styles et al.*, 2014]. Therefore, the reinjecton of water ($2.85 \cdot 10^6$ m^3 between 1993 and 2012) below the water oil contact of the reservoir is not considered as a possible triggering mechanism. For our modeling approach, we consider a flat reservoir depletion layer at 3 km depth assuming an average pore pressure reduction of 1 MPa over a period of 32 years and uncertainties with 5% and 95% percentiles at 0.5 MPa and 5 MPa, respectively. The report of *Styles et al.* [2014] indicates that the pore pressure drop may have reached locally a value of 4 MPa at maximum. We assume similar elastic parameter

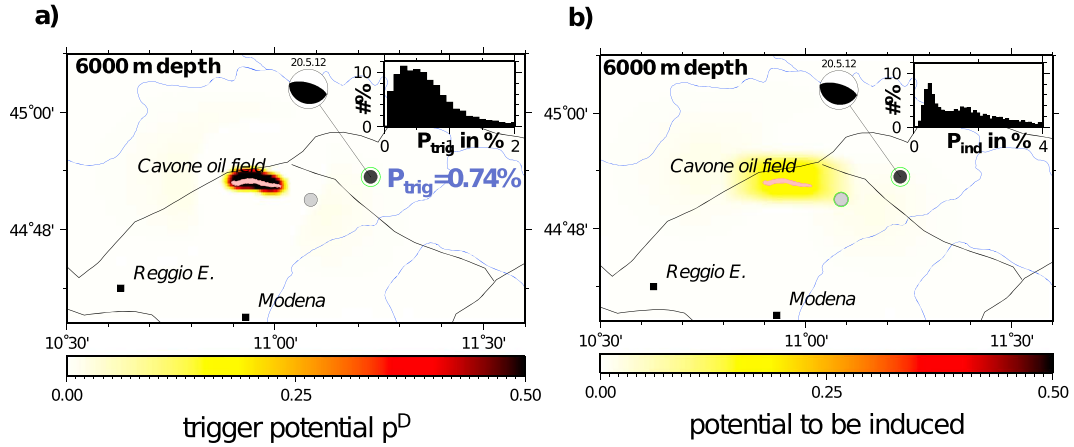

Figure 9. (a) The trigger potential at 6 km depth from depletion of the Cavone oil field (colored grid) is plotted together with the location (black filled circle, location uncertainties in green) and source mechanism of the main shock from 10 May 2012 (M_W 6.1). The largest aftershock (M_W 5.9) is indicated by the grey filled circle. The trigger potential for thrust faulting mechanism is largest beneath the Cavone oil field (pink filled polygon). Mapped faults are plotted as solid lines. The inlet figures show the frequency distribution of P_{trig} at the epicenter. (b) Colored grid shows the potential that earthquakes are induced assuming a fault filter dimension of $15 \times 8 \times 8$ km^3. The probability to induce a M_W 6.1 earthquake is at the hypocenter < 1% and even at the oil field < 50%.

as for the other case studies, i.e., Lamé's parameter of 12 GPa, a field thickness of 600 m and an effective uniaxial compaction coefficient of $c_m = 0.533$.

Figure 9a shows the spatial distribution of the estimated trigger potential together with the contour line of the 1σ error ellipse of the location uncertainty of the main shock in the layer of hypocenter at 7 km depth. The potential p^D is nearly zero in the regions outside the oil field where the earthquakes occur. For comparison, the position of the largest aftershock is also plotted. Consequently, we derive a trigger probability of $P_{\text{trig}} \approx 0.007$, with a narrow distribution of errors. The low potential to have been triggered can be expected, since the earthquake is relatively far from the field. Additionally, thrust faulting mechanisms are unfavorably oriented in the volume outside the field and favorably oriented above and below the depleted field. Therefore, p^D is large in the region directly beneath the oil field.

Figure 9b shows trigger probability for the test whether the Emilia earthquake was induced. We observe again the effect that the potential function is smoothed out and reduced in its absolute level. However, the probability that the event could have been induced is still small and below 2% on average.

4. Discussion

The examples in the previous chapter demonstrate the discrimination approach for specific input parameter. In order to exploit the uncertainties, input parameters have been varied uniformly or according to a normal distribution (for location) and the bootstrap results were statistically analyzed. Therefore, the effects of uncertainties were considered.

The trigger probability is controlled by the ratio $\dot{\tau}^D/\dot{\tau}^T$, which depends on background seismicity, reservoir field parameter, and elastic modules.

The possible range of $\dot{\tau}^T$ as a function of background seismicity (e.g., estimated by means of a and b values, maximal magnitudes, or thickness of the seismogenic crust) has been discussed in Table 2. The possible range of $\dot{\tau}^D$ can be studied by means of elastic field parameter or pore pressure reduction. As may be expected, the varying of elastic parameter of the crust within a reasonable range leads to relatively small effects, especially if the depletion model is calibrated by measured surface subsidence. However, a large sensitivity is observed if the pore pressure reduction is varied. This parameter is also difficult to obtain and often bears large uncertainties. We so far assumed a pore pressure reduction ΔP in the Ekofisk oil field in 2001 of about 47 MPa and of about 10 MPa in the Rotenburg gas field in 2004, respectively. For Emilia, we used a pore pressure drop of only 1 MPa. While a pore pressure drop of 47 MPa is quite remarkable (although well confirmed for Ekofisk), a drop of 10 MPa over a production period of more than 22 years

is quite reasonable if compared to other gas fields. For the bootstrap error analysis ΔP was varied with 5% and 95% percentile intervals of [44 MPa; 50 MPa], [5 MPa; 20 MPa], and [0.5 MPa; 5 MPa] for Ekofisk, Rotenburg/Söhlingen, and Emilia/Cavone, respectively.

For Ekofisk both P_{trig} and P_{ind} vary only slightly and are above 74%, in spite the assumption that input parameters were varied. It seems that the Ekofisk earthquake is a clear case of a triggered and depletion-induced event. From 1999 to 2002 a volume of $\approx 1.9 \cdot 10^6$ m^3 of water was injected between 1830 and 2134 m in the northern part of the field, very likely because of a disrupted well casing. This is of interest for the triggered-induced discussion. The injection occurred in the depth of the future subhorizontal rupture plane under high overpressure above the tensile strength of the shale and mud rocks [*Ottemöller et al.*, 2005]. This enabled the formation of a horizontal hydrofracture, as indicated from the 10–15 cm uplift of the seafloor over an area of about 1×1 km^2. It possibly triggered the seismic rupture of the M_W 4.3 earthquake [*Ottemöller et al.*, 2005; *Cesca et al.*, 2011]. For instance, in Oklahoma between 1993 and 2011 about $1.5 \cdot 10^5$ m^3 of waste water was injected in an old, sealed reservoir in about 2 km depth. This likely triggered a sequence of three $M_W > 5$ earthquakes in 2011 on a nearby subvertical fault with preexisting, tectonic stress, the largest having a magnitude of M_W 5.6 [*Keranen et al.*, 2013]. Although the overpressure and the total volume of injected water was even larger for Ekofisk, the story is not as simple. Waste water injections in depleted reservoirs are routinely performed without triggering significant earthquakes, may be because preexisting faults with accumulated tectonic shear stress are not available. For instance, at the oil field in Hamburg Sinstorf, Germany, about $1 \cdot 10^6$ m^3 of waste water were injected between 1995 and 2015 without any felt earthquake so far. Different to these cases, the injection at Ekofisk occured in a sedimentary layer above the reservoir. At this depth at the border of the reservoir, subhorizontal planes accumulated sufficient shear stress from the previous production. It is therefore possible that the hydrofracture propagated subhorizontally in its original plane until the region under high shear stress was hit so that shear rupture could be triggered. We do not attempt to estimate the trigger potential from the water injection separately for two reasons: first, this would not change the main conclusion and second, even without the unintended water injection, the depletion-induced shear stress was sufficient to explain a triggering role for this earthquake.

For the Rotenburg earthquake the probabilities are generally smaller. P_{trig} is about 71%. P_{ind}, however, is smaller and close to 50%. The smaller probability would indicate that the rupture was partly driven by tectonic stress already prone on a preexisting fault.

For the Emilia earthquake, both the trigger and the induced case probability are very small and nearly zero. The Emilia M_W 6.1 main shock cannot originate from depletion-induced stress rate of the Cavone oil field and must have been triggered and controlled by tectonic stress on a preexisting fault. This is widely in accordance with the conclusions of *Styles et al.* [2014], who assessed it as highly unlikely that exploitation at Mirandola may have produced sufficient stress change to generate an induced event. *Styles et al.* [2014] do not exclude at 100% a possible anthropogenic contribution for event triggering, since the role of the fluids in the reservoir and the surrounding rocks have not been included in the estimates (no hydraulic connection to fault). The reinjection of water below the water oil contact during production reduces the pressure drop in the reservoir, which results in a smaller depletion effect with respect to the production-based estimate. Therefore, our probability calculation represents a worst-case estimate.

In our approach to analyze the induced potential, a possible problem may arise if the human loading (field depletion) is occurring only for a short time. For an induced earthquake, according to *McGarr and Simpson* [1997], most of the coseismic stress release should have been provided by accumulated, human-induced stress. For the presented applications we evaluate stress rates from depletion over several decades. Therefore, it was justified to assume steady state loading rates and that a sufficient amount of stress has been accumulated. For instance, a depletion-induced stress rate of 120 kPa/yr at the border of the Ekofisk field acting over a production period of more than 30 years accumulates easily to a Coulomb stress of more than 3.6 MPa. Stress drop of shallow earthquakes ranges between 0.1 and 30 MPa and can be explained by the accumulated human-induced stress. However, if shorter periods of loading are evaluated, the absolute value of accumulated stress resolved on the fault should be considered in the discussion.

Another discussion may concern the simplified depletion model, following the strain nuclei method proposed by *Geertsma* [1973]. It is important to note that the proposed discrimination approach is independent on the specific modeling technique and thus other, more sophisticated modeling may be incorporated

in future. However, we feel that the boundary element (BE) method adapted here is sufficient for a reasonable estimate and may be taken as a first choice. First-order effects, as the extent and shape of the gas and oil field and the free-surface effect, are well considered. The estimated stress changes are quite good approximations in some distance from the reservoir but may be biased very close to the boundary of the field. However, close the field the stresses are highest and the triggering problem is not very disputed, if an earthquake appears to be located in this high-stress region. Another advantage of the BE approach is that interacting fields can easily be considered and that even large areas of several tens of kilometers can be handled with a standard PC or notebook. On the other hand, effects from elastic stratification, field compartments, or 3-D structures are not included in the stress modeling.

The proposed scheme is flexible and can be adapted to different cases. For instance, the consideration of depth-dependent tectonic stress rates (or alternatively depth-dependent background seismicity) can be easily considered. The size of the earthquakes under study can be considered by means of adaption of the fault filter for smoothing. The lack of knowledge of the earthquake depth or location can be easily included by means of an appropriate pdf of the location uncertainty.

The source mechanism is another issue that may be discussed. For instance, if the earthquake source mechanism is in accord with the tectonic background stress, and the earthquake rupture is favorably oriented, the earthquake was potentially tectonic induced. On the other hand, if the source mechanism is opposed to the tectonic stress, the likelihood to be depletion induced should be increased. Our proposed scheme considers the source mechanism since stress rates, both for the tectonic background stress and for the depletion-induced stress, are estimated in rupture direction on the plane of the assumed earthquake fault. Unfavorable oriented rupture slip would implicitly result in very small tectonic stress rates and thus lead to larger trigger probabilities than favorably oriented ruptures.

Earthquake-earthquake interaction, for instance, between aftershocks or between main shock and aftershock, is well-known phenomena. The stress perturbation generated by the previous event may trigger the following event. Our method, as it is formulated here, does not consider stress perturbations from previous earthquakes. If trigger probabilities for aftershocks shall be estimated, e.g., for Rotenburg or Emilia aftershocks, an extension of the scheme to include time dependency and earthquake-induced Coulomb stress changes is needed.

Political authorities, insurance companies, and other end users may use the results of the discrimination study for their regulations of individual cases. Other potential applications may concern hazard or risk studies. For this, the method needs to be extended to be able to consider many scenarios so that the probabilistic results may be used as a prognostic tool. In such a case the method can be combined with other discriminators or expert knowledge. A Bayesian approach would be straight forward for such an attempt, since the result is already probabilistic and therefore easily implemented in a Bayesian scheme. *Passarelli et al.* [2013] and *Cesca et al.* [2013a] give examples for the consideration of a prior distribution.

5. Conclusions

We propose a method to estimate the probability that an isolated earthquake in proximity to a gas or oil field was depletion triggered or depletion induced. The discrimination is given in a probabilistic sense, stating the likelihood to have been related to the depletion-induced stress perturbations. The method distinguishes depletion-triggered and depletion-induced earthquakes, and it is the first time a probabilistic discrimination scheme is suggested to distinguish these types of earthquake ruptures. The method is flexible and can be adapted to different problems and case studies. All input parameters are given, and the results are reproducible. Uncertainties of input parameters can easily be considered. The probabilistic discrimination may help both, industry and public stakeholders, to analyze the triggering problem in an objective and reproducible way.

We demonstrate the method by three case studies. The first event has a magnitude of M_W 4.3 and occurred close to the Ekofisk oil field (North Sea). We show that this earthquake, which was very shallow and located above the oil field, was depletion triggered and also depletion induced with a high probability. The second event occurred close to the Söhlingen gas field in North Germany. It has a magnitude of M_W 4.4 and occurred below the reservoir level slightly outside the border field. Its mechanism was favorable of being triggered at the position of the hypocenter. Our method indicates that the event was triggered with a

probability of about 74% and induced with a probability of about 50%. The third case study concerns a M_W 6.1 thrust faulting event in the Po Plain in Northern Italy. The oil field is located about 20 km from the hypocenter and additionally experienced only a minor pore pressure reduction during the lifetime of its production. Further, the mechanism of the earthquake was unfavorably oriented for being depletion triggered. Our discrimination scheme clearly indicates that the Emilia earthquake was neither triggered nor induced by field depletion. It is very likely that the Emilia North Italy earthquake was exclusively of tectonic origin.

Appendix A: Boundary Element Modeling of Field Depletion

Geertsma [1973] derived analytical solutions to estimate surface subsidence as a response to production-induced compaction of disk-shaped undrained reservoirs. The analytical solutions have been extended by *Segall* [1992] to calculate displacement and stress beneath the surface, and both solutions have been applied to different cases as, for instance, the subsidence pattern above the Groningen field in Netherland [e.g., *Van Hasselt*, 1992] or induced seismicity in the region of the Lacq gas field, France [e.g., *Grasso*, 1992].

Other studies applied finite element techniques (FE) to analyze the mechanical behavior of reservoir depletion and induced seismicity [e.g., *Mulders*, 2003]. *Chan* [2004] used a 3-D boundary element (BE) method to estimate the land subsidence caused by large volume production of fields in Louisiana, including thereby the effect of inelastic deformation on nearby faults. The BE method of Chan, however, did not consider the behavior of a porous reservoir formation but prescribed a compaction displacement at the upper sealing layer of the field only.

In our work we modify an in-house developed 3-D BE method to account for poroelastic field behavior. Although simulation tools of similar power may be available by means of complex FE 3-D modeling, the approach proposed here requires only few discretization elements and is thus efficient. This allows to consider field depletion in a large region and to account for field-field and field-fault interaction.

We extended the displacement discontinuity method of *Crouch and Starfield* [1983] to 3-D problems [*Thorwart*, 2001]. Green function solutions for rectangular elements (subfaults) with constant slip are taken from *Okada* [1992]. The method has previously been used to understand dislocation problems of earthquake faults or fluid-filled fracture emplacement [*Thorwart*, 2001].

The reservoir is discretized by rectangular boundary elements of constant size. On each BE a constant dislocation δu^n in normal direction and δu^t and δu^s in north (tangential) and east shear directions (shear) is assumed, respectively. On each element, shear and normal traction can be prescribed, and normal and tangential displacement is inverted for assuming a homogeneous elastic half-space.

As demonstrated by *Geertsma* [1973], the displacement field from a depleting, sealed, and infinitely thin porous reservoir can be represented by an integral over nuclei of strain solutions, if scaled with prefactor $4\pi/c_m$, where $c_m = \alpha(1-2\nu)^2/(2\nu(1-\nu^2))$ is the effective uniaxial compaction coefficient. We approximate the Green function of a nuclei of strain from a pore pressure reduction ΔP in the field formation by a sum over three tensile sources, which are orthogonal to each other and are loaded by normal traction equal to ΔP. This ad hoc implementation has the advantage to directly apply a BE method previously developed and calibrated for crack and fault problems loaded by shear and normal traction.

The method reproduces well the theoretical predictions of known analytical solutions, e.g., the subsidence and emplacement of a superficial and/or deep disk-shaped reservoir embedded in an elastic half-space (Figure A1), even at subparallel planes as close as half of the thickness of the reservoir. The accuracy of the BE solution may be improved by finer discretization if needed.

The compaction in Figure A1 shows that both surfaces of the reservoir subside as a consequence of pore pressure reduction. This is different to typical tensile crack solutions and can be viewed as a free-surface effect, since the overall stiffness of the effective media is reduced by the pore pressure depletion in the field. The subsidence of the upper surface is larger than the subsidence of the lower sealing surface (Figure A1), indicating that the field is actually compacted.

Knowing the displacement solution of the compaction problem, the stress tensor at each point in the half-space can be efficiently calculated by the conventional BE approach. The BE modeling is fast and may easily cover a region of large extent and several separated fields, which are possibly interacting. The method can incorporate the effect of nearby, possibly growing faults or uneven field depletion.

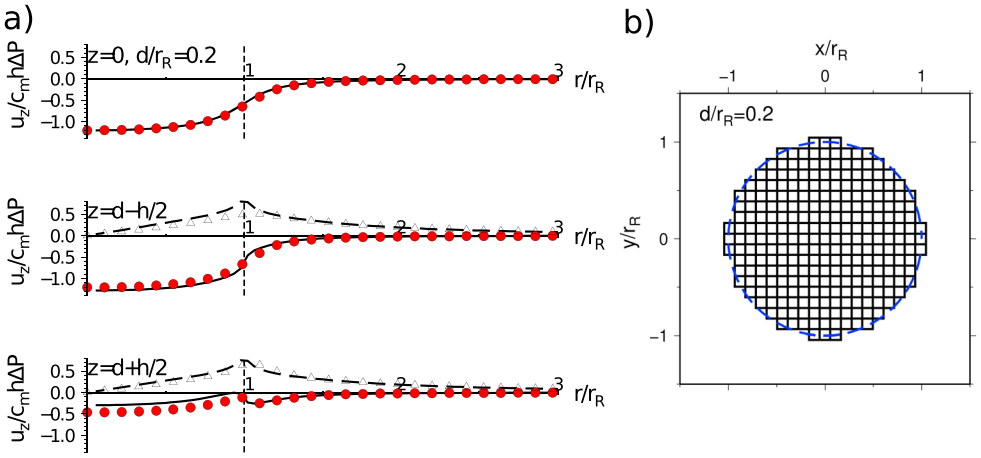

Figure A1. Verification of the nuclei of strain approach of the 3-D boundary element method for a disk-shaped reservoir of radius r_R in depth $d = 0.2r_R$ embedded in an elastic half-space. (a) Comparison of the displacement field at the surface and in depth levels $d \pm h/2$, where h is the assumed thickness of the field. Solid and dashed lines indicate the vertical and radial analytical displacement of *Geertsma* [1973], respectively. The filled circles and triangles give the approximate solution of the BE method. Shear module and Poisson ratio were set to 12 GPa and 0.25. The assumed pore pressure reduction was 30 MPa in a porous layer of $h = 200$ m thickness and with Biot-Willies constant of $\alpha = 1$. The effective uniaxial compaction coefficient is $c_m = \alpha(1-2\nu)^2/(2\nu(1-\nu^2))$. (b) Plane view on the disk-shaped reservoir with rectangular BE elements.

Appendix B: Pore Pressure at Field Depth From Gas Volume Production

The discovered gas fields in North Germany are mostly hosted within the Rotliegend sandstone or the Zechstein formation. The Rotliegend fields have a typical depth between 5 and 4 km. Oldest fields have been exploited since 1975. The most productive on-shore fields in Germany in 2004 were Söhlingen (cumulative production since 1982 of $31.6 \cdot 10^9$ m^3), Rotenburg (cumulative production since 1986 of $39.9 \cdot 10^9$ m^3), and Völkersen (cumulative production since 1994 of $8.04 \cdot 10^9$ m^3) [e.g., *Pasternak et al.*, 2004].

The measured pore pressure changes ΔP or other production parameter are not available to us. The normalized cumulative production is therefore used to estimate ΔP at the depth of the formation rocks. It is well known that pore pressure decrease in a field linearly follows the depletion trend of that field [e.g., *Van Eijs et al.*, 2006; *Mulders*, 2003, Figure 7.24 or P/Z plots]. The cumulative production ΔV_0 is measured under atmospheric pressure $P_0 = P(0) = 0.1$ MPa and at a temperature of $T_0 = 273°$ K. The depletion volume at the depth of the gas-liquid transition is then

$$\Delta V = \frac{P_0\, T_c}{P_c\, T_0}\Delta V_0\,, \tag{B1}$$

where we assume $T_c \approx 471$ K and $P_c \approx 4.637$ MPa [e.g., *Barberii*, 1989]. The pore pressure change at the depth of the field due to the depletion of liquid gas with volume ΔV and a bulk modulus of $K_l \approx 1$ GPa [e.g., *Lumley*, 1994, expanded abstract SEG] is

$$\begin{aligned}\Delta P(z) &= -K_l\,\frac{\Delta V}{V_p} = -K_l\,\frac{P_0 T_c}{P_c T_0}\,\frac{\Delta V_0}{\Phi\, h\, A}\\ &= -K_l\,\frac{P_0 T_c}{P_c T_0 \Phi}\,\frac{\Delta h_0}{h},\end{aligned} \tag{B2}$$

where h is the average thickness of the field and $\Phi_p = V_p/V_{\text{total}} = V_p/(hA)$ is the porosity of the reservoir formation. Equation (B2)

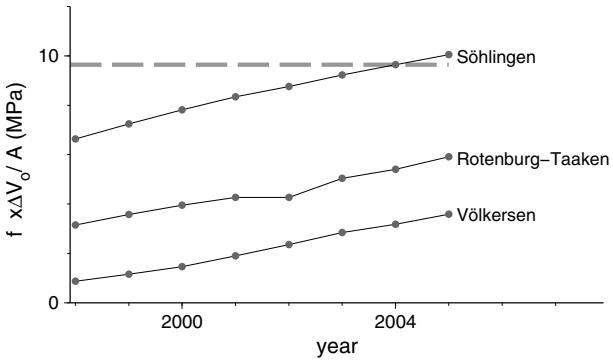

Figure B1. Cumulative production ΔV_0 normalized by field area A since 1999 for the three Rotliegend fields Rotenburg, Söhlingen, and Völkersen. The normalization factor is $f = \frac{K_l P_0 T_c}{P_c T_0 \Phi_p h}$, where $P_0 = 0.1$ MPa, $T_0 = 273$ K, $P_c = 46$ MPa, $T_c = 471$ K, $h = 200$ m, $\Phi_p = 0.1$, and $K_l = 1$ GPa have been used. The horizontal line indicates the value reached by the Söhlingen field in 2004.

is used to estimate the pore pressure change ΔP in fields under production. Assuming $h \approx 200$ m and $\Phi \approx 20\%$, a pore pressure change of the Söhlingen field in year 2004 after 22 years of production was about $\Delta P \approx 10$ MPa (Figure B1). This roughly corresponds to an estimated pressure change rate of 1 MPa in 2 years for fields in the Rotliegend (R. Van Eijs, personal communication, 2007) and is after 20 years in the range of observed pore pressure changes in fields in Netherlands when first triggered earthquakes have occurred [e.g., *Van Eijs et al.*, 2006].

Acknowledgments
Comments from the Associate Editors and two reviewers helped improve the manuscript and were appreciated. We thank Sebastian Heimann for some help with python scripting and Matthias Holschneider for discussions of the probabilistic concept. Figures were prepared using GMT (Wessel, P. and W. H. F. Smith, Free software helps map and display data, EOS Trans. AGU, 72, 441, 1991). S.C. was funded by the MINE project (BMBF German Ministry of Education and Research, Programme GEOTECHNOLOGIEN, grant of project BMBF03G0737). Data sources are referenced in the text.

References

Abdulraheem, A., M. Zaman, and J.-C. Roegiers (1994), A finite-element model for Ekofisk field subsidence, *J. Pet. Sci. Eng.*, *10*, 299–310.
Baldschuh, R., U. Fritsch, and F. Kockel (2001), The basement block pattern in Northwest Germany, in *Geotektonischer Atlas von Nordwest-Deutschland und dem Deutschen Nordsee-Sektor*, edited by R. Baldschuh et al., cartographic map, 1:500,000, Schweitzerbart.
Barberii, E. (1989), *El Pozo Ilustrado, PDVSA*, 1–600 pp., Ediciones Foncied, Caracas-Venezuela.
Basili, R., P. Burrato, and G. Valensise (2001), Slow active faults in compressional settings. Methodologies, results and source parameters on sites—The Po Plain, *SAFE Project Final Rep. Deliverable 4.6c and 8.1*, EU Project SAFE.
Basili, R., P. Valensise, G. Vannoli, P. Burrato, U. Fracassi, S. Mariano, M. Tiberti, and E. Boschi (2008), Characterizing swells in the southern Pacific from seismic and infrasound noise analysis, *Tectonophysics*, *453*, 20–43, doi:10.1016/j.tecto.2007.04.014.
Blaser, L., F. Krüger, M. Ohrnberger, and F. Scherbaum (2010), Scaling relations of earthquake source parameter estimates with special focus on subduction environment, *Bull. Seismol. Soc. Am.*, *100*, 2912–2926, doi:10.1785/0120100111.
Bossu, R. (1996), Etude de la sismicité intraplaque de la région de Gazli (Ouzbékistan) et localisation de la déformation sismique, PhD thesis, Université Joseph-Fourier Grenoble, Grenoble, France.
Brückner-Röhling, S., S. Fleig, H. Forsbach, F. Kockel, P. Krull, and H. Wirth (2004), The movement phases of tectonic faults in the Tertiary period of Northern Germany—Results of structure-geological investigations, *Z. Geol. Wiss.*, *5–6*, 295–231.
Bungum, H., A. Alsaker, L. Kvamme, and R. Hansen (1991), Seismicity and seismotectonics of Norway and nearby continental shelf areas, *J. Geophys. Res.*, *96*, 2249–2265.
Bungum, H., C. Lindholm, A. Dahle, G. Woo, F. Nadim, J. Holme, O. Gudmestad, T. Hagberg, and K. K. Karthigeyan (2000), New seismic zoning maps for Norway, the North Sea, and the United Kingdom, *Seismol. Res. Lett.*, *71*, 687–697.
Burrato, P., L. Cucci, and G. Valensise (2003), An inventory of river anomalies in the Po Plain, Northern Italy: Evidence for active blind thrust faulting, *Ann. Geophys.*, *46*(5), 865–882.
Catalli, F., M. Cocco, R. Console, and L. Chiaraluce (2008), Modeling seismicity rate changes during the 1997 Umbria-Marche sequence (central Italy) through rate- and state-dependent model, *J. Geophys. Res.*, *113*, B11301, doi:10.1029/2007JB005356.
Cesca, S., S. Heimann, K. Stammler, and T. Dahm (2010), Automated procedure for point and kinematic source inversion at regional distances, *J. Geophys. Res.*, *115*, B06304, doi:10.1029/2009JB006450.
Cesca, S., T. Dahm, K. Juretzek, and D. Kühn (2011), Rupture process of the 7 May 2011, M_w 4.2, Ekofisk induced earthquake, *Geophys. J. Int.*, *187*, 407–413, doi:10.1111/j.1365-246X.2011.05151.x.
Cesca, S., A. Rohr, and T. Dahm (2013a), Discrimination of induced seismicity by full moment tensor inversion and decomposition, *J. Seismolog.*, *17*, 147–163, doi:10.1007/s10950-012-9305-8.
Cesca, S., B. Dost, and A. Oth (2013b), Preface to the special issue "Triggered and induced seismicity: Probabilities and discrimination", *J. Seismolog.*, *17*, 1–4, doi:10.1007/s10,950-012-9338-z.
Cesca, S., T. Braun, F. Maccaferri, L. Passarelli, E. Rivalta, and T. Dahm (2013c), Source modelling of the *M*5-6 Emilia-Romagna, Italy, earthquakes (2012 May 20–29), *Geophys. J. Int.*, *193*, 1658–1672, doi:10.1093/gji/ggt069.
Cesca, S., F. Grigoli, S. Heimann, A. Gonzalez, E. Buforn, S. Maghsoudi, E. Blanch, and T. Dahm (2014), The September–October 2013 seismic sequence offshore Spain: A case of seismicity triggered by gas injection?, *Geophys. J. Int.*, *198*, 941–953.
Chan, A. (2004), Production induced reservoir compaction, permeability loss and land surface subsidence, PhD thesis, Stanford Univ., Stanford, Calif.
Crouch, S., and A. Starfield (1983), *Boundary Element Methods in Solid Mechanics*, 321 pp., George Allen and Unwin Ltd, London.
Dahm, T., F. Krüger, K. Stammler, K. Klinge, R. Kind, K. Wylegalla, and J. Grasso (2007), The $M_W = 4.4$ Rotenburg, Northern Germany, earthquake and its possible relationship with gas recovery, *Bull. Seismol. Soc. Am.*, *97*, 691–704, doi:10.1785/0120050149.
Dahm, T., et al. (2010), How to discriminate induced, triggered and natural seismicity?, in *Proceedings of the Workshop Induced Seismicity, November 15–17, 2010*, edited by A. Oth, and J. Ritter, European Center for Geodynamics and Seismology, Luxemburg.
Dahm, T., et al. (2013), Recommendation for the discrimination of human-related and natural seismicity, *J. Seismolog.*, *17*, 197–202, doi:10.1007/s10950-012-9295-6.
Davis, S., P. Nyffenegger, and C. Frohlich (1995), The 9 April 1993 earthquake in south-central Texas: Was it induced by fluid withdrawal?, *Bull. Seismol. Soc. Am.*, *85*, 1888–1896.
Davis, S. D., and C. Frohlich (1993), Did (or will) fluid injection cause earthquakes? Criteria for a rational assessment, *Seismol. Res. Lett.*, *64*, 207–224.
Dieterich, J. (1994), A constitutive law for rate of earthquake production and its application to earthquake clustering, *J. Geophys. Res.*, *99*, 2601–618.
Dieterich, J. (1995), Earthquake simulation with time-dependent nucleation and long-range interactions, *Nonlinear Process. Geophys.*, *2*, 109–120.
Ellsworth, W. (2013), Injection-induced earthquakes, *Science*, *341*, 7 pp., doi:10.1126/science.1225942.
Geertsma, J. (1973), A basic theory of subsidence due to reservoir compaction: The homogeneous case, *Verhandelingen Kon. Ned. Geol. Mijnbouwk. Gen.*, *28*, 43–62.
Giardini, D., et al. (2013), Seismic Hazard Harmonization in Europe (SHARE), Online data resource, Swiss Seismol. Serv., ETH Zurich, Zurich, Switzerland, doi:10.12686/SED-00000001-SHARE.
Grasso, J. (1992), Mechanics of seismic instability induced by the recovery of hydrocarbons, *Pure Appl. Geophys.*, *139*, 507–543.
Grünthal, G., and W. Minkley (2005), Bergbauinduzierte seismische Aktivität als Quelle seismischer Belastungen—Zur Notwendigkeit der Ergänzung der Karte der Erdbebenzonen der DIN 4149, *Bautechnik*, *82*, 508–513, doi:10.1002/bate.200590167.
Grünthal, G., and R. Wahlström (2012), The European-Mediterranean Earthquake Catalogue (EMEC) for the last millennium, *J. Seismolog.*, *16*, 535–557, doi:10.1007/s10950-012-9302-y.

Grünthal, G., R. Arvidsson, and C. C. Bosse (2010), Earthquake model for the European-Mediterranean region for the purpose of GEM1, *Sci. Tech. Rep. STR10/04*, Deutsches GeoForschungsZentrum GFZ, Potsdam, doi:10.2312/GFZ.b103-10043.

Gupta, H. (2002), A review of recent studies of triggered earthquakes by artificial water reservoirs with special emphasis on earthquakes in Koyna, India, *Earth Sci. Rev.*, *58*, 279–310.

Hainzl, S., G. Brietzke, and G. Zoeller (2010), Quantitative earthquake forecasts resulting from static stress triggering, *J. Geophys. Res.*, *115*, B11311, doi:10.1029/2010JB007473.

Keranen, K., H. Savage, G. Abers, and E. Cochran (2013), Potentially induced earthquakes in Oklahoma, USA: Links between wastewater injection and the 2011 M_W 5.7 earthquake sequence, *Geology*, *41*, 699, doi:10.1130/G34045.1.

Kostrov, B. (1974), Seismic moment and energy of earthquakes, and seismic flow of rock, *Izv. Acad. Sci. USSR Phys. Solid Earth*, *1*, 23–40.

Lumley, D., A. Nur, S. Strandenes, J. Dvorkin, and J. Packwood (1994), Seismic monitoring of oil production: A feasibility study, Stanford Exploration Project, Rep. 80, pp. 1–259, SEG Conf., Los Angeles, 15 May 2001.

McGarr, A. (1991), On a possible connection between three major earthquakes in California and oil production, *Bull. Seismol. Soc. Am.*, *81*, 948–970.

McGarr, A., and D. Simpson (1997), Keynote lecture: A broad look at induced and triggered seismicity, in *Rockbursts and Seismicity in Mines*, edited by S. J. Gibowitz, and S. Lasocki, pp. 948–970, Balkema, Rotterdam.

McGarr, A., D. Simpson, and L. Seeber (2002), Case histories of induced and triggered seismicity, in *International Handbook of Earthquake and Engineering Seismology*, vol. 81A, edited by W. W. Lee et al., pp. 647–661, Acad. Press, San Diego, Calif.

Meletti, C., V. D'Amico, G. Ameri, A. Rovida, and M. Stucchi (2012), Seismic hazard in the Po Plain and the 2012 Emilia earthquakes, *Ann. Geophys.*, *55*(4), 623–629, doi:10.4401/ag-6158.

Mulders, F. (2003), Modelling stress development and fault slip in and around a producing gas reservoir, PhD thesis, TU Delft, Netherlands.

Okada, Y. (1992), Internal deformation due to shear and tensile faults in a half-space, *Bull. Seismol. Soc. Am.*, *82*, 1018–1040.

Ottemöller, L., H. Nielsen, K. Atakan, J. Braunmiller, and J. Havskov (2005), The 7 May 2001 induced seismic event in the Ekofisk oil field, North Sea, *J. Geophys. Res.*, *110*, B10301, doi:10.1029/2004JB003374.

Passarelli, L., F. Maccaferri, E. Rivalta, T. Dahm, and E. Abebe Boku (2013), A probabilistic approach for the classification of earthquakes as "triggered" or "not triggered": Application to the 1975 Krafla diking event followed by the 13th Jan 1976 M 6.2 earthquake on the Tjörnes Fracture Zone, Iceland, *J. Seismolog.*, *17*, 165–187, doi:10.1007/s10950-012-9289-4.

Pasternak, M., S. Brinkmann, J. Messner, and R. Sedlacek (2004), *Erdöl und Erdgas in der Bundesrepublik Deutschland*. Niedersächisches Landesamt für Bodenforschung, Jahresbericht, pp. 1–45.

Segall, P. (1992), Induced stresses due to fluid extraction from axisymmetric reservoirs, *Pure Appl. Geophys.*, *139*, 4535–4560.

Shapiro, S., O. S. Krüger, and C. Dinske (2013), Probability of inducing given-magnitude earthquakes by perturbing finite volumes of rocks, *J. Geophys. Res. Solid Earth*, *118*, 3557–3575, doi:10.1002/jgrb.50264.

Styles, P., P. Gasparini, E. Huenges, P. Scandone, S. Lasocki, and F. Terlizzese (2014), *Report on the Hydrocarbon Exploration and Seismicity in Emilia Region*, International Commissikon on Hydrocarbon Exploration and Seismicity in the Emilia Region (ICHESE) February, pp. 1–213.

Thorwart, M. (2001), *3D-Randelementmethode zur Simulation von Faults und Rissen im Halbraum*.

Van Eijs, R., F. Mulders, M. Nepveu, C. Kenter, and B. Scheffers (2006), Correlation between hydrocarbon reservoir properties and induced seismicity in the Netherlands, *Eng. Geol.*, *84*, 99–111, doi:10.1016/j.enggeo.2006.01.002.

Van Hasselt, J. (1992), Reservoir compaction and surface subsidence resulting from oil and gas production, *Geol. Mijnbouw*, *71*, 107–118.

Wells, D., and C. Coppersmith (1994), New empirical relationship among magnitude, rupture length, rupture width, rupture area and surface displacement, *Bull. Seismol. Soc. Am.*, *84*, 974–1002.

Zhuang, J., and Y. Ogata (2004), Analyzing earthquake clustering features by using stochastic reconstruction, *J. Geophys. Res.*, *109*, B05301, doi:10.1029/2003JB002879.